Improving Heat Exchanger Effectiveness in Industrial Applications Through Nanofluid Utilization

Chetan Somani[1*], Jagdish S. Talpada[2], Jiva G. Kuchhadiya[3]
Department of Mechanical Engineering, Polytechnic
The Maharaja Sayajirao University of Baroda, Vadodara
Corresponding Author Email[1]: somani.chetan-polymed@msubaroda.ac.in*

Abstract

Low thermal conductivity in conventional heat transfer fluids limits the efficiency and compactness of industrial thermal systems. This study experimentally investigates the convective heat transfer and thermodynamic performance of a 2 m galvanized iron concentric tube-in-tube double-pipe heat exchanger (DPHE) using an Al_2O_3–water nanofluid. The nanofluid was synthesized using a stable two-step method by dispersing 25 g of alumina nanoparticles (20–30 nm) into 25 L of deionized water with polyvinyl alcohol (PVA) surfactant under ultrasonic sonication. Experiments were conducted at fixed inlet temperatures and constant mass flow rates for both parallel-flow and counter-flow configurations. The baseline water-to-water performance was directly compared with the water-to-nanofluid system.

In the parallel-flow configuration, the nanofluid increased the heat transfer rate by 65% (from 0.2283 to 0.3780 kW) and enhanced the overall heat transfer coefficients by approximately 45%, resulting in a 50% improvement in thermal effectiveness (from 0.181 to 0.272). In the counter-flow arrangement, the nanofluid improved the heat transfer rate by 33% (from 0.4496 to 0.5995 kW), increased the overall heat transfer coefficients by 7.8%, and raised the effectiveness to a peak value of 0.363.

The results further demonstrate that incorporating the Al_2O_3 nanofluid in a parallel-flow configuration can achieve thermal performance comparable to that of a conventional water-based counter-flow system. This finding highlights a practical approach for improving compact thermal equipment where counter-current flow arrangements are restricted by spatial or structural limitations.

Keywords: Nanofluids; Heat exchangers; Thermal conductivity; Al_2O_3 nanoparticles

1. Introduction

Industrial thermal processing and energy conversion systems rely heavily on the efficient operation of heat exchangers to maximize productivity and minimize fuel consumption. Traditional heat transfer fluids, such as water and various oils, possess inherently low thermal conductivity, which creates a major bottleneck in advancing thermal system performance. The integration of nanotechnology through colloidal suspensions known as nanofluids offers a highly promising pathway to overcome these thermodynamic limitations and transform next-generation heat exchange technology.

1.1 Background

Modern manufacturing, power generation, and chemical processing facilities depend directly on the efficacy of thermal transport components like evaporators, condensers, and boilers. Over the past decades, standard engineering modifications—such as extending surface areas, adding macro-baffles, or altering flow geometries—have reached a point of diminishing returns. As a result, contemporary research focus has shifted from structural optimization to modifying the thermophysical properties of the transport medium itself.

Nanofluids represent a major breakthrough in this domain, created by dispersing nanometer-sized particles (typically metals, metallic oxides, or carbon structures) uniformly within conventional base fluids. Because solid materials exhibit thermal conductivities that are orders of magnitude higher than standard liquids, their stable suspension alters the fundamental transport characteristics of the host fluid. This advanced formulation enhances the convective heat transfer coefficient and effective thermal conductivity, offering a compact and scalable strategy to reduce the physical footprint of industrial machinery while cutting energy consumption.

1.2 Previous Study

The empirical foundation of nanofluid performance has been established across diverse flow regimes and equipment designs. Han [1] pioneered the synthesis of advanced nanofluid systems using semiconductor nanorods and phase-change nanodroplets, reporting thermal conductivity increases up to 52% and latent heat-driven capacity gains up to 126%, confirming that nanoscale dispersion alters standard effective medium predictions. Computational fluid dynamics (CFD) modeling has validated these behaviors under laminar flow conditions; simulations of Al2O3/water mixtures in circular tubes [4] show that reducing nanoparticle diameters from 50 nm to 20 nm yields higher heat transfer coefficients, which scale proportionally with the Reynolds number and particle concentration. Similarly, Ting and Hou [7] demonstrated a 25.5% convective heat transfer enhancement using 2.5 vol.% Al_2O_3 in a square cross-section duct, noting that the thermal enhancement far exceeded the fluid's independent thermal conductivity increase (9.98%).
Experimental validation across various industrial heat exchanger geometries demonstrates clear thermal benefits alongside predictable hydraulic penalties:

Tubular and Coiled Configurations: Mukeshkumar et al. [2] tested Al_2O_3/water nanofluids in a shell and helically coiled tube exchanger under turbulent conditions, achieving tube-side Nusselt number increases up to 56% at a 0.8% volume fraction due to secondary flow formations, accompanied by a modest 9% pressure drop. Albadr et al. [3] observed similar upward trends in horizontal shell-and-tube setups, noting that convective coefficients increased alongside mass flow rates and volume fractions. Double-tube, shell-and-tube, and coiled designs were further reviewed by Singh and Sarkar [14], who affirmed widespread efficiency gains but highlighted high material costs and long payback periods as ongoing commercial hurdles.

Plate and Finned Equipment: Taghizadeh-Tabari et al. [12] introduced TiO_2 nanoparticles into plate heat exchangers (PHE) for milk pasteurization, utilizing a performance index to show that the convective gains outweighed the frictional pumping penalties. Kadhim et al. [8] successfully enhanced cross-flow dynamics in an integral finned-tube heat exchanger using 40 nm MgO particles dispersed in distilled water. Comprehensive reviews by Gupta et al. [9, 10] consolidated these findings, noting that across plate and shell-and-tube configurations, nanofluids consistently cut down equipment size, reduced thermal processing times, and improved overall energy efficiency.

Microchannels and Baffles: Advanced hydrodynamic optimizations have also been pursued. Hasan [5] evaluated Diamond-water and Al_2O_3-water coolants in micro pin fin heat sinks under laminar regimes (Re 100–900), discovering that while heat dissipation increased across square, triangular, and circular fin geometries, fluid friction rose concurrently. To mitigate these penalties, Bahiraei et al. [11] employed neural network modeling and multi-objective optimization on shell-and-tube exchangers fitted with helical baffles. Their work proved that adjusting the helix angle and baffle overlap allows high-concentration nanofluids to operate efficiently even when low pressure drops are prioritized.

1.3 Research Gap

Despite extensive research into the performance of nanofluids at low to moderate operating temperatures ($T \leq 100$ °C) using standard water, glycol, or basic oil matrices, there is a clear shortage of data regarding high-temperature applications. Industrial environments like oil and gas refineries, petrochemical plants, and heavy thermal power networks regularly operate at extreme temperatures, yet high-temperature thermal oils have been largely ignored in nanofluid research. Barai et al. [13] highlighted critical structural challenges that worsen under harsh operational states, including particle sedimentation, clogging, chemical instability, and system erosion at higher volume fractions.

While Safaei et al. [15] demonstrated that adding low-concentration (0.1 wt%) SiO_2 and Al_2O_3 nanoparticles to specialized high-temperature fluids like Therminol 66 could boost heat exchanger efficiency by up to 88% within the 280°C to 320°C range without destabilizing viscosity, a broad understanding of long-term stability, optimum particle blending, and multi-objective optimization under these harsh conditions remains undeveloped. Consequently, more research is needed to evaluate the interaction between advanced nanoparticle suspensions and high-temperature base oils to ensure stable, long-term performance in high-intensity industrial environments.

1.4 Contribution of this study

While the convective benefits of nanoscale suspensions have been documented in conventional water-based systems, this work addresses important gaps in practical implementation and comparative performance evaluation. The major contributions of this research are summarized as follows:

Direct Flow Regime Comparison: This study presents a direct experimental comparison of Al_2O_3-water nanofluid performance under identical mass flow conditions for both parallel-flow and counter-flow configurations within the same DPHE.

Quantification of Low-Concentration Enhancements: The study demonstrates that a stable low-concentration nanofluid formulation (25 g of 20–30 nm nanoparticles dispersed in 25 L of deionized water) can produce significant thermal enhancement, including a 65% increase in parallel-flow heat transfer rate and a 50% improvement in heat exchanger effectiveness, without requiring complex chemical treatment or excessive pumping power.

Overcoming Parallel-Flow Limitations: The experimental results show that integrating nanofluid into a conventional parallel-flow arrangement enables the system to achieve thermal effectiveness comparable to that of a standard water-to-water counter-flow configuration ($\varepsilon = 0.272$). This provides a practical solution for industrial applications where space limitations restrict the use of counter-flow piping arrangements.

Figure 1. *Setup of Double Pipe Heat Exchanger test rig*

2. Experimental set up and procedure

The experimental apparatus is constructed around a concentric tube-in-tube heat exchanger design. In this configuration, the hot thermal medium—consisting of water heated via an electric geyser—circulates through the inner tube, while the cooling medium travels through the outer annular space. The flow rate of the hot water loop is tightly regulated via a dedicated control valve to maintain a consistent directional flow.

To evaluate different hydrodynamic profiles, the cold water loop is equipped with a versatile valve manifold that allows the fluid to be introduced at either end of the annulus. This setup enables the system to alternate seamlessly between parallel-flow and counter-flow operating modes through precise valve actions, as illustrated in Figure 1.

The experimental trials were conducted under constant flow rate conditions across both parallel-flow and counter-flow arrangements. Fluid temperatures at the key inlets and outlets were quantified using high-accuracy glass thermometers filled with mercury or alcohol, while the volumetric flow rates were verified using a calibrated graduated measuring flask paired with a digital stopwatch. To ensure data accuracy, all operational parameters were logged only after the system reached a verified thermal steady state. Furthermore, the outer boundary of the annulus was wrapped in a dual-layer insulation system—comprising an inner layer of thermocol and an external layer of asbestos—to minimize parasitic heat losses to the ambient surroundings.

Table 1. *Geometric specifications of the experimental DPHE*

Component	Parameter	Dimension
Inner Tube (Hot Loop)	Inner Diameter (di)	8.10 mm
	Outer Diameter (do)	13.44 mm
Outer Tube (Cold Annulus)	Inner Diameter (Di)	27.50 mm
	Outer Diameter (Do)	33.80 mm
Heat Exchanger	Effective Length (L)	2.00 m

2.1 Instrumentation and Specifications

The experimental double-pipe heat exchanger (DPHE) is fabricated from galvanized iron (G.I.) piping with the specific geometric dimensions outlined in Table 1.

Thermal measurements at all critical inlet and outlet junctions were captured using precision glass thermometers with an operational range of 0°C to

100°C. The volumetric and mass flow rates of both the hot and cold fluid streams were quantified using a 1000 cc graduated measuring flask combined with a digital stopwatch. Thermal input for the hot water loop was supplied and regulated by a 3 kW electric geyser (manufactured by Bajaj Electricals). To ensure adiabatic operating conditions along the test section, the outer surface of the exterior G.I. pipe was thoroughly wrapped in a thick layer of thermocol insulation.

2.2 Experimental procedure

The experiment was initially conducted using water as both the hot and cold working fluids. Thermometers were positioned at the designated inlet and outlet locations, and the initial readings were recorded at room temperature. The flow on the hot water side was started first, followed by the initiation of flow through the annulus, and the heat exchanger was operated under parallel flow configuration. Subsequently, the electric geyser was switched on to heat the hot water stream.

The flow rates on both the hot and cold water sides were adjusted and maintained at the desired values. Temperature readings for both streams were recorded only after steady-state conditions were achieved. Care was taken to maintain constant and accurately measured flow rates throughout the experiment. The same experimental procedure was repeated for the counter-flow configuration under identical operating conditions.

After completing the tests with pure water, experiments were performed using water–nanofluid mixtures under the same flow conditions and operational procedure. The nanofluid was prepared using the method proposed by Jung et al. Initially, Polyvinyl Alcohol (PVA) and Al_2O_3 nanoparticles (SLR Ltd., Mumbai, India) with an average particle diameter of 20–30 nm were mixed with deionized (DI) water. The prepared mixture was then sonicated using an ultrasonic disruptor to obtain a stable nanofluid suspension. The volume fraction of nanoparticles was maintained equal to that of PVA. In the present work, the nanofluid was prepared by dispersing 25 g of Al_2O_3 nanoparticles in 25 liters of DI water.

3. Experimental Analysis and Data Reduction

This section presents the experimental data gathered from the testing campaigns along with the mathematical formulations utilized to evaluate the thermal response profiles. To minimize errors and guarantee consistency, all thermophysical properties of the fluids were analyzed at their relevant bulk mean temperatures.

3.1 Baseline System Verification (Pure Water)

To validate the experimental setup and establish a reference benchmark for subsequent nanofluid analysis, the initial experiments were conducted using pure water as both the hot and cold working fluids. During these baseline trials, steady and controlled mass flow rates were maintained throughout the operation.

The stabilized flow parameters recorded during the reference experiments are summarized below:

- Hot fluid mass flow rate: 0.0375 kg/s (flowing through the inner G.I. tube)
- Cold fluid mass flow rate: 0.0340 kg/s (flowing through the outer annular section)

The observed steady-state temperature distribution metrics across both parallel and counter-flow modes are detailed in Table 2.

Table 2. *Observation parameters for the DPHE without nanofluid*

Type of flow	Hot Water Side		Cold Water Side	
	Inlet Temp. (T_{hi}) °C	Outlet Temp. (T_{ho}) °C	Inlet Temp. (T_{ci}) °C	Outlet Temp. (T_{co}) °C
Parallel flow	49	47	38	39
Counter flow	49	46	38	41

3.2 Evaluation Methodology for Water-to-Water Baseline

The thermal parameters derived from the pure water experimental runs were evaluated using standard engineering formulations as detailed below:

3.2.1 Parallel Flow Regime

(i) Heat transfer rate (q), is calculated as q_h = Heat transfer rate from hot water

$$q_h = m_h \times C_{ph} \times (T_{hi} - T_{ho}) \quad (1)$$

Assume $C_{ph} = C_{pc} = 4.187$ kJ/kg-K, $q_h = 0.3140$ kW, q_c = Heat transfer rate to the cold water

$$q_c = m_c \times C_{pc} \times (T_{co} - T_{ci}) \quad (2)$$

Where $q_c = 0.1427$ kW and $q = \left(\frac{q_h + q_c}{2}\right)$

Therefore, q = 0.2283 kW

The Logarithmic Mean Temperature Difference (LMTD) is derived via the boundary temperature drops:

$$LMTD = \Delta T_m = \frac{\Delta T_i - \Delta T_o}{\log_e\left(\frac{\Delta T_i}{\Delta T_o}\right)} \quad (4)$$

And its value is = 9.42 ^{0}C.

Using Newton's law of cooling, the total thermal transmission performance is calculated from the active inner pipe area,

$$q = U \times A \times \Delta T_m \quad (5)$$

Therefore, $U = \frac{q}{A} \times \Delta T_m$

The calculated inner overall heat transfer coefficient (U_{ri}) and outer overall heat transfer coefficient (U_{ro}) are:

$$U_{ri} = \frac{q}{A_i} \times \Delta T_m \quad (6)$$

where, $A_i = \pi \times d_i \times l$

U_{ri} = 42.29 kW-K/m^2

Outer overall heat transfer coefficient, U_{ro} is calculate by

$$U_{ro} = \frac{q}{A_o} \times \Delta T_m \quad (7)$$

where, $A_o = \pi \times d_o \times l$

U_{ro} = 25.49 kW-K/m^2

The effectiveness ε of the transport network is determined using the minimum heat capacity rate (C_{ph}):

The effectiveness of the heat exchanger can be calculated by using the expression:

$$\varepsilon = \frac{m_h \times C_{ph} \times (T_{hi} - T_{ho})}{m_h \times C_{ph} \times (T_{hi} - T_{ci})} \quad (8)$$

and it is equal to 0.181.

3.2.2 Counter Flow Regime

Using identical thermal evaluation metrics, the energy profiles extracted for the counter-flow baseline configuration are:

q_h = Heat transfer rate from hot water

$$q_h = m_h \times C_{ph} \times (T_{hi} - T_{ho}) \quad (9)$$

Assume $C_{ph} = C_{pc} = 4.187$ kJ/kg-K, $q_h = 0.4710$ kW and q_c = Heat transfer rate to the cold water

$$q_c = m_c \times C_{pc} \times (T_{co} - T_{ci}) \quad (10)$$

$q_c = 0.4282$ kW

$$q = \left(\frac{q_h + q_c}{2}\right)$$

q = 0.4496 kW

LMTD can be calculated as

$$LMTD = \Delta T_m = \frac{\Delta T_i - \Delta T_o}{\log_e\left(\frac{\Delta T_i}{\Delta T_o}\right)} \quad (11)$$

It's calculated value is as 7.60 ^{0}C

Overall heat transfer coefficient can be calculated by using,

$$q = U \times A \times \Delta T_m \quad (12)$$

Therefore, $U = \frac{q}{A} \times \Delta T_m$

Inner overall heat transfer coefficient, U_{ri} is calculate by

$$U_{ri} = \frac{q}{A_i} \times \Delta T_m \quad (13)$$

where, $A_i = \pi \times d_i \times l$, U_{ri} =67.26 kW-K/m^2

Outer overall heat transfer coefficient, U_{ro} is calculate by

$$U_{ro} = \frac{q}{A_o} \times \Delta T_m \quad (14)$$

where, $A_o = \pi \times d_o \times l$, U_{ro} =40.53 kW-K/m^2

The effectiveness of the heat exchanger can be calculated by using the expression:

$$\varepsilon = \frac{m_h \times C_{ph} \times (T_{hi} - T_{ho})}{m_h \times C_{ph} \times (T_{hi} - T_{ci})} \quad (15)$$

The obtained value is s 0.272.

3.3 Experimental Evaluation with Al_2O_3-Water Nanofluid

The following observations were achieved by trial of double pipe heat exchanger with water as hot and cold fluid.

Observations:

Flow rate (m_h) of hot water side: 0.0375 kg/sec

Flow rate (m_c) of cold water side: 0.0340 kg/sec

The steady-state temperatures recorded for the nanofluid operation are organized in Table 3.

Table 3. *Observation parameters for the DPHE with nanofluid*.

Type of flow	Hot Water Side		Cold Water Side	
	Inlet Temp. (T_{hi}) ^oC	Outlet Temp. (T_{ho}) ^oC	Inlet Temp. (T_{ci}) ^oC	Outlet Temp. (T_{co}) ^oC
Parallel flow	49	46	38	40
Counter flow	49	45	38	42

3.4 Evaluation Methodology for Nanofluid Performance

The thermal performance of the DPHE was evaluated by comparing the experimental results obtained using pure water and Al_2O_3-water nanofluid under identical operating conditions. Key performance parameters such as heat transfer rate, overall heat transfer coefficient, LMTD, and heat exchanger effectiveness were calculated and analyzed for both parallel-flow and counter-flow configurations.

3.4.1 Parallel Flow Regime

Evaluating the energy equation yields a substantial enhancement in thermal flux using the nanoparticle suspension:

Heat transfer rate (q), is calculated as q_h = Heat transfer rate from hot water

$$q_h = m_h \times C_{ph} \times (T_{hi} - T_{ho}) \quad (16)$$

Assume $C_{ph} = C_{pc}$ = 4.187 kJ/kg-K, q_h = 0.471 kW, q_c = Heat transfer rate to the cold water

$$q_c = m_c \times C_{pc} \times (T_{co} - T_{ci}) \quad (17)$$

q_c = 0.285 kW

$$q = \left(\frac{q_h + q_c}{2} \right)$$

q = 0.378 kW

LMTD can be calculated as

$$LMTD = \Delta T_m = \frac{\Delta T_i - \Delta T_o}{\log_e \left(\frac{\Delta T_i}{\Delta T_o} \right)} \quad (18)$$

LMTD = 8.24 ^{0}C

Overall heat transfer coefficient can be calculated by using,

$$q = U \times A \times \Delta T_m \quad (19)$$

Therefore, $U = \frac{q}{A} \times \Delta T_m$

Inner overall heat transfer coefficient, U_{ri} is calculate by

$$U_{ri} = \frac{q}{A_i} \times \Delta T_m \quad (20)$$

where, $A_i = \pi \times d_i \times l$

U_{ri} = 61.33 kW-K/m^2

Outer overall heat transfer coefficient, U_{ro} is calculate by

$$U_{ro} = \frac{q}{A_o} \times \Delta T_m \quad (21)$$

where, $A_o = \pi \times d_o \times l$

U_{ro} = 36.96 kW-K/m^2

The effectiveness of the heat exchanger can be calculated by using the expression:

$$\varepsilon = \frac{m_h \times C_{ph} \times (T_{hi} - T_{ho})}{m_h \times C_{ph} \times (T_{hi} - T_{ci})} \quad (22)$$

ε = 0.272

3.4.2 Counter Flow Regime

The maximum thermal performance metrics were achieved when combining the counter-current arrangement with the Al_2O_3 suspension:

Heat transfer rate (q), is calculated as
q_h = Heat transfer rate from hot water

$$q_h = m_h \times C_{ph} \times (T_{hi} - T_{ho}) \quad (23)$$

Assume $C_{ph} = C_{pc}$ = 4.187 kJ/kg-K, q_h = 0.6280 kW, q_c = Heat transfer rate to the cold water

$$q_c = m_c \times C_{pc} \times (T_{co} - T_{ci}) \quad (24)$$

q_c = 0.5709 kW

$$q = \left(\frac{q_h + q_c}{2} \right)$$

q = 0.5995 kW

LMTD can be calculated as

$$LMTD = \Delta T_m = \frac{\Delta T_i - \Delta T_o}{\log_e \left(\frac{\Delta T_i}{\Delta T_o} \right)} \quad (25)$$

LMTD = 6.15 ^{0}C

Overall heat transfer coefficient can be calculated by using,

$$q = U \times A \times \Delta T_m \quad (26)$$

Therefore, $U = \frac{q}{A} \times \Delta T_m$

Inner overall heat transfer coefficient, U_{ri} is calculate by

$$U_{ri} = \frac{q}{A_i} \times \Delta T_m \quad (27)$$

where, $A_i = \pi \times d_i \times l$, U_{ri} = 72.56 kW-K/m^2

Outer overall heat transfer coefficient, U_{ro} is calculate by

$$U_{ro} = \frac{q}{A_o} \times \Delta T_m \quad (28)$$

where, $A_o = \pi \times d_o \times l$, U_{ro} = 43.73 kW-K/m^2

The effectiveness of the heat exchanger can be calculated by using the expression:

$$\varepsilon = \frac{m_h \times C_{ph} \times (T_{hi} - T_{ho})}{m_h \times C_{ph} \times (T_{hi} - T_{ci})} \quad (29)$$

The calculated value is equal to 0.363.

4. Results and discussion

The inlet temperatures for the fluid loops were recorded as Tci = 311 K (38°C) for the cold stream and Thi = 322 K (49°C) for the hot stream. Two distinct structural arrangements—parallel-flow and counter-flow—were systematically evaluated. The initial experimental matrix was performed using the water-water configuration to establish baseline parameters and was subsequently repeated under identical operating conditions for the water-nanofluid configuration.

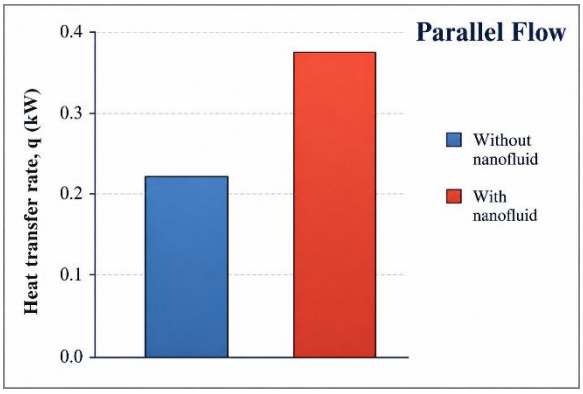

Figure 2: *Comparison of heat transfer rate for parallel flow*

4.1 Parametric Performance Analysis (Parallel Flow Regime)

The performance shifts observed during parallel flow operation reveal substantial thermal improvements when the system transitions from pure water to the nanoparticle suspension. Figure 2 illustrates the distinct heat transfer rate (q) profiles within the DPHE for both the baseline water–water configuration and the enhanced water–nanofluid configuration under parallel flow conditions.

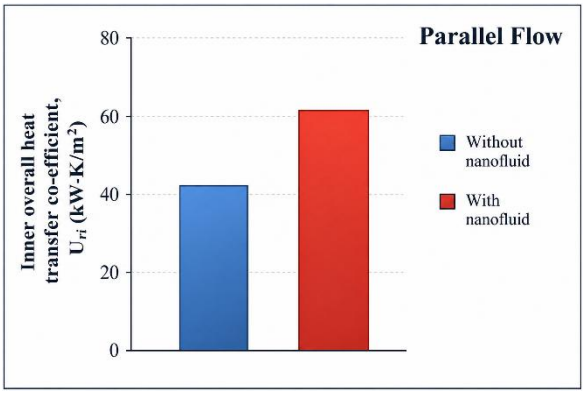

Figure 3: *Comparison of inner overall heat transfer co-efficient for parallel flow*

The experimental data indicates that utilizing the Al_2O_3-water nanofluid as the cooling medium results in a 65% increase in the total heat transmission rate compared to the pure water baseline. This sharp increase is driven by the enhanced thermal conductivity of the suspension and increased micro-convection effects caused by chaotic nanoparticle interactions within the boundary layers. Figures 3 and 4 provide a comparative analysis of the inner and outer overall heat transfer coefficients for the parallel-flow arrangement.

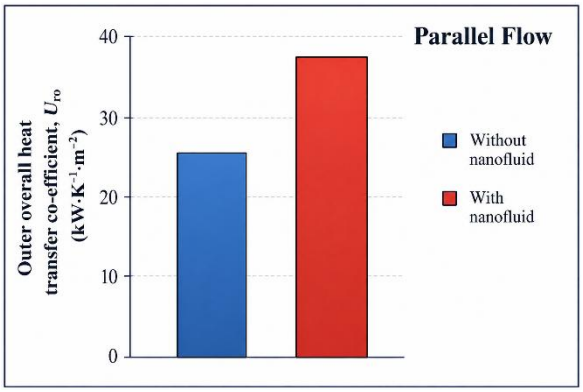

Figure 4: *Comparison of outer overall heat transfer co-efficient for parallel flow.*

The calculated results show that the inner overall heat transfer coefficient (Uri) increases by 45%, while the outer overall heat transfer coefficient (Uro) shows a corresponding improvement of 44%. These nearly uniform increases across both fluid boundaries confirm that the thermal resistance of the system drops significantly when nanoparticles are introduced into the annular stream. Figure 5 highlights the resulting impact on the thermal performance metrics of the system, demonstrating that the overall effectiveness (ε) of the DPHE during parallel flow increases by 50% when utilizing the nanofluid.

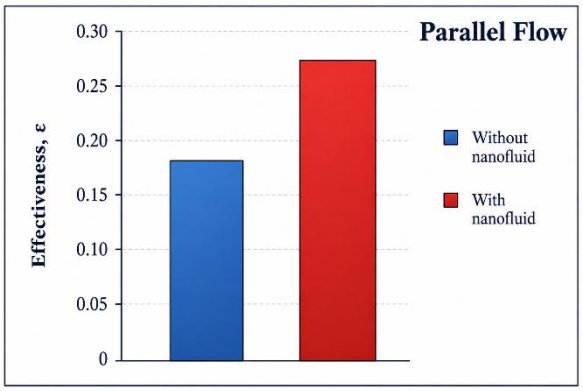

Figure 5: *Comparison of effectiveness for parallel flow.*

This substantial improvement shows that modifying the transport properties of the fluid allows a standard parallel-flow arrangement to achieve thermal extraction efficiencies that would typically require larger equipment sizes or more complex flow configurations.

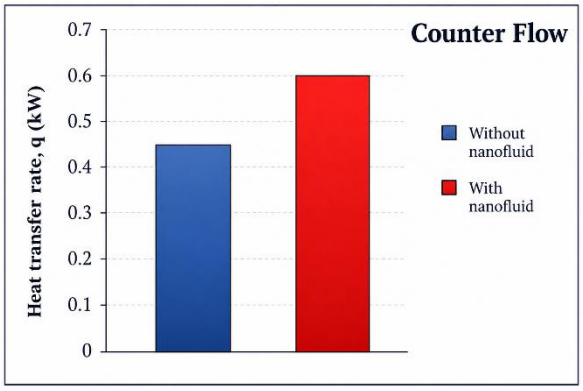

Figure 6: *Comparison of heat transfer rate for counter flow*

4.2 Parametric Performance Analysis (Counter Flow Regime)

The counter-flow regime was evaluated under identical mass flow and inlet temperature boundary conditions to isolate the geometric impacts of counter-current fluid paths paired with nanotechnology. Figure 6 presents the comparative profiles of the heat transfer rate (q) for both the conventional water–water run and the enhanced water–nanofluid run under counter-flow conditions.

The empirical data reveals that the heat transmission rate is augmented by 33% when the nanoparticle suspension is introduced. Although the percentage increase is lower than that seen in the parallel flow configuration, the counter-flow matrix yields the highest absolute energy transfer rate (0.5995 kW) achieved across the entire testing campaign. Figures 7 and 8 present the comparative values of the inner and outer overall heat transfer coefficients within the counter-flow configuration, repsectively.

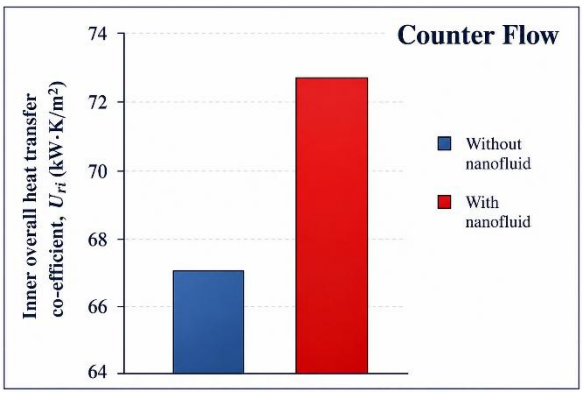

Figure 7: *Comparison of inner overall heat transfer co-efficient for counter flow.*

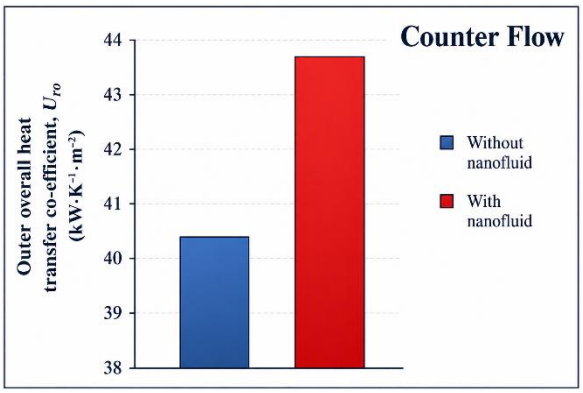

Figure 8: *Comparison of outer overall heat transfer co-efficient for counter flow.*

The analytical data indicates an enhancement of 7.8% for both the inner overall heat transfer coefficient (Uri) and the outer overall heat transfer coefficient (Uro). Because the baseline counter-flow configuration with pure water is already highly efficient, the relative margin of improvement for the convective coefficients is smaller, although it still provides a valuable thermal advantage. Figure 9 presents the calculated system effectiveness trends across the counter-flow testing runs.

Reflecting the improvements observed in total energy transmission, the thermal effectiveness of the DPHE increases by 34% when utilizing the nanofluid medium. This improvement allows the system to achieve a peak operational effectiveness value of 0.363, establishing the combination of an engineered colloidal suspension and a counter-current flow pattern as the optimal configuration for this heat exchange network.

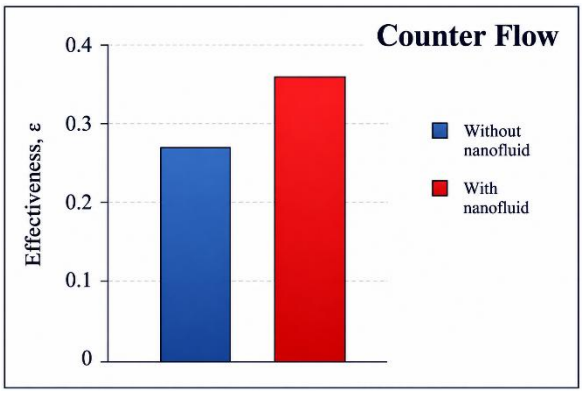

Figure 9: *Comparison of effectiveness for counter flow*

5. Conclusion

The thermal performance and energy conversion efficacy of a G.I. double-pipe tube-in-tube heat exchanger were systematically evaluated using pure water and a low-concentration Al_2O_3–water nanofluid. The primary conclusions derived from the experimental data and thermodynamic analysis are as follows:

Enhancement of Thermal Energy Transmission: Dispersing 20–30 nm alumina nanoparticles into the annular cooling loop significantly increased heat transfer rates across both flow configurations. In the parallel-flow regime, the heat transfer rate increased by 65% (from 0.2283 to 0.3780 kW), while in the counter-flow regime, it increased by 33% (from 0.4496 to 0.5995 kW). The combination of counter-flow arrangement and nanoparticle suspension produced the highest thermal dissipation achieved in this study (0.5995 kW).

Reduction of System Thermal Resistance: The overall heat transfer coefficients showed a substantial increase, indicating that the nanofluid effectively reduced thermal resistance within the boundary layer. For parallel-flow operation, the inner and outer overall heat transfer coefficients improved by 45% and 44%, respectively. Under counter-flow conditions, both coefficients increased by 7.8%.

Augmentation of Thermodynamic Effectiveness: The heat exchanger effectiveness closely followed the enhancement in convective heat transfer. The effectiveness of the parallel-flow configuration increased by 50% (from 0.181 to 0.272), while the counter-flow configuration exhibited a 34% improvement, reaching a maximum value of 0.363.

Overcoming Structural Limitations: A significant finding of this work is that employing a low-concentration Al_2O_3 nanofluid in a parallel-flow configuration can achieve thermal effectiveness comparable to that of a conventional water-based counter-flow system (effectiveness = 0.272). This demonstrates a practical solution for enhancing heat transfer performance in compact industrial systems where counter-flow arrangements are structurally constrained.

Underlying Transport Mechanisms: The observed thermal enhancement is primarily attributed to the increased effective thermal conductivity of the nanofluid, combined with localized micro-convection and boundary layer disturbance caused by the Brownian motion of suspended nanoparticles within the base fluid.

Future research may investigate the use of alternative nanofluids, such as CuO–water nanofluids, to further

enhance the thermal performance of DPHEs. Additional studies can also explore the effects of different pipe materials, heat exchanger geometries, and nanoparticle volume concentrations on heat transfer characteristics and overall thermodynamic performance. Furthermore, investigations involving hybrid nanofluids, long-term stability analysis, pressure drop behavior, and pumping power requirements could provide deeper insight into the practical industrial applicability of nanofluid-based heat exchangers

Refrences

[1] Han, Z. (2008). *Nanofluids with Enhanced Thermal Transport Properties* (Doctoral dissertation, University of Maryland, College Park).

[2] Mukeshkumar, P. C., et al. (2012). Experimental study on parallel and counter flow configuration of a shell and helically coiled tube heat exchanger using Al_2O_3/water nanofluid. *Journal of Materials and Environmental Science*, 3(4), 766–775.

[3] Albadr, J., Tayal, S., & Alasadi, M. (2013). Heat transfer through heat exchanger using Al_2O_3 nanofluid at different concentrations. *Case Studies in Thermal Engineering*, 1(1), 38–44.

[4] [Author details not fully provided in abstract] (2013). The CFD simulation of heat transfer characteristics of a nanofluid in a circular tube under constant heat flux using Fluent software in the laminar flow.

[5] Hasan, M. I. (2014). Investigation of flow and heat transfer characteristics in micro pin fin heat sink with nanofluid. *Applied Thermal Engineering*, 63(2), 598–607.

[6] Nawras, A. A. (2014). *Heat Transfer Enhancement in a Uniformly Heated Tube Using Nanofluids* (Master's thesis, University of Babylon).

[7] Ting, H. H., & Hou, S. S. (2015). Investigation of laminar convective heat transfer for Al_2O_3-water nanofluids flowing through a square cross-section duct with a constant heat flux. *Materials*, 8(8), 5321–5335.

[8] Kadhim, Z. K., Kassim, M. S., & Abdul Hassan, A. Y. (2016). Effect of MgO nanofluid on heat transfer characteristics for integral finned tube heat exchanger. *International Journal of Mechanical Engineering and Technology*, 7(2), 11–24.

[9] Gupta, S. K., Verma, H., & Yadav, N. (2022). A review on recent development of nanofluid utilization in shell & tube heat exchanger for saving of energy. *Materials Today: Proceedings*, 54, 579–589.

[10] Gupta, S. K., et al. (2021). A review on recent advances and applications of nanofluids in plate heat exchanger. *Materials Today: Proceedings*, 44, 229–241.

[11] Bahiraei, M., Hangi, M., & Saeedan, M. (2015). A novel application for energy efficiency improvement using nanofluid in shell and tube heat exchanger equipped with helical baffles. *Energy*, 93, 2229–2240.

[12] Taghizadeh-Tabari, Z., et al. (2016). The study on application of TiO_2/water nanofluid in plate heat exchanger of milk pasteurization industries. *Renewable and Sustainable Energy Reviews*, 58, 1318–1326.

[13] Barai, R., Kumar, D., & Wankhade, A. (2021). Heat transfer performance of nanofluids in heat exchanger: a review. *Journal of Thermal Engineering*, 9(1), 86–106.

[14] Singh, S. K., & Sarkar, J. (2020). Improvement in energy performance of tubular heat exchangers using nanofluids: a review. *Current Nanoscience*, 16(2), 136–156.

[15] Safaei, A., Hossein Nezhad, A., & Rashidi, A. (2020). High temperature nanofluids based on Therminol 66 for improving the heat exchangers power in gas refineries. *Applied Thermal Engineering*, 170, 114991.